JACS
JOURNAL OF THE AMERICAN CHEMICAL SOCIETY
pubs.acs.org/JACS
Article

Isoreticular Contraction of Cage-like Metal−Organic Frameworks with Optimized Pore Space for Enhanced C_2H_2/CO_2 and C_2H_2/C_2H_4 Separations

Lei Zhang,* Taotao Xiao, Xiayun Zeng, Jianjun You, Ziyu He, Cheng-Xia Chen,* Qianting Wang, Ayman Nafady, Abdullah M. Al-Enizi, and Shengqian Ma*

Cite This: J. Am. Chem. Soc. 2024, 146, 7341−7351

Read Online

ACCESS | Metrics & More | Article Recommendations | Supporting Information

ABSTRACT: The C_2H_2 separation from CO_2 and C_2H_4 is of great importance yet highly challenging in the petrochemical industry, owing to their similar physical and chemical properties. Herein, the pore nanospace engineering of cage-like mixed-ligand MFOF-1 has been accomplished via contracting the size of the pyridine- and carboxylic acid-functionalized linkers and introducing a fluoride- and sulfate-bridging cobalt cluster, based on a reticular chemistry strategy. Compared with the prototypical MFOF-1, the constructed FJUT-1 with the same topology presents significantly improved C_2H_2 adsorption capacity, and selective C_2H_2 separation performance due to the reduced cage cavity size, functionalized pore surface, and appropriate pore volume. The introduction of fluoride- and sulfate-bridging cubane-type tetranuclear cobalt clusters bestows FJUT-1 with exceptional chemical stability under harsh conditions while providing multiple potential C_2H_2 binding sites, thus rendering the adequate ability for practical C_2H_2 separation application as confirmed by the dynamic breakthrough experiments under dry and humid conditions. Additionally, the distinct binding mechanism is suggested by theoretical calculations in which the multiple supramolecular interactions involving C−H···O, C−H···F, and other van der Waals forces play a critical role in the selective C_2H_2 separation.

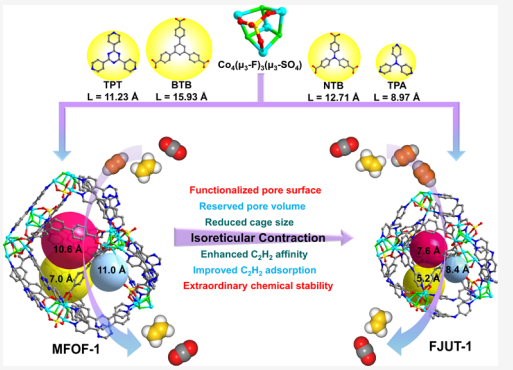

INTRODUCTION

As two important chemical feedstocks, acetylene (C_2H_2) and ethylene (C_2H_4) have been widely used to produce various downstream chemical commodities, such as acrylic acid, vinyl chloride, polyethylene, and ethynyl alcohols. In industry, C_2H_2 is usually produced by the combustion of natural gas or thermal cracking of hydrocarbons, accomplished with a substantial amount of CO_2 impurities,[1,2] while C_2H_4 is afforded through the steam cracking of hydrocarbons, accompanied by a small amount of C_2H_2 byproduct.[3,4] In addition, C_2H_2 with high reactivity, flammability, and explosiveness can cause some undesired reactions or notorious industrial manufacturing processes. For instance, trace C_2H_2 can poison the catalyst by forming metal acetylides during ethylene polymerization. Therefore, the selective C_2H_2 separation from CO_2 and C_2H_4 is of great importance to obtain poly grade C_2H_2 and C_2H_4 feedstocks for highly safe and efficient production of chemicals. The separation or purification of C_2H_2 from CO_2 and C_2H_4 is typically realized through cryogenic distillation or solvent extraction in industry, involving intensive cost and energy consumption owing to their similar boiling points (boiling point: 189.3 K for C_2H_2, 194.7 K for CO_2, and 169.5 K for C_2H_4), which has spurred the development of more efficient technology as alternatives to achieve this daunting challenge.[5−7]

At present, adsorptive separation technology based on porous solid materials has been proven to be one of the most promising approaches due to its energy efficiency and its being environmentally friendly. However, the similar physicochemical properties of C_2H_2, CO_2, and C_2H_4 (kinetic diameter: 3.3 Å for C_2H_2 and CO_2, 4.2 Å for C_2H_4; quadrupole moment: 7.2×10^{26} e.s.u. cm^2 for C_2H_2, 4.3×10^{26} e.s.u. cm^2 for CO_2, 1.5×10^{26} e.s.u. cm^2 for C_2H_4; polarizability: $33.3-39.3 \times 10^{25}$ cm^3 for C_2H_2, 29.11×10^{25} cm^3 for CO_2, 42.5×10^{25} cm^3 for C_2H_4; Table S1) pose a significant challenge to develop highly efficient adsorbents for C_2H_2/CO_2 and C_2H_2/C_2H_4 separations through physical adsorption mechanism.[8−12]

In light of the tunable pore size/shape/volume,[13−16] and functionable pore surface,[17−21] metal−organic frameworks (MOFs), emerging as a new class of porous solid materials, have attracted a lot of attention in the field of gas adsorption and

Received: October 28, 2023
Revised: February 20, 2024
Accepted: February 23, 2024
Published: March 5, 2024

https://doi.org/10.1021/jacs.3c12032
J. Am. Chem. Soc. 2024, 146, 7341−7351

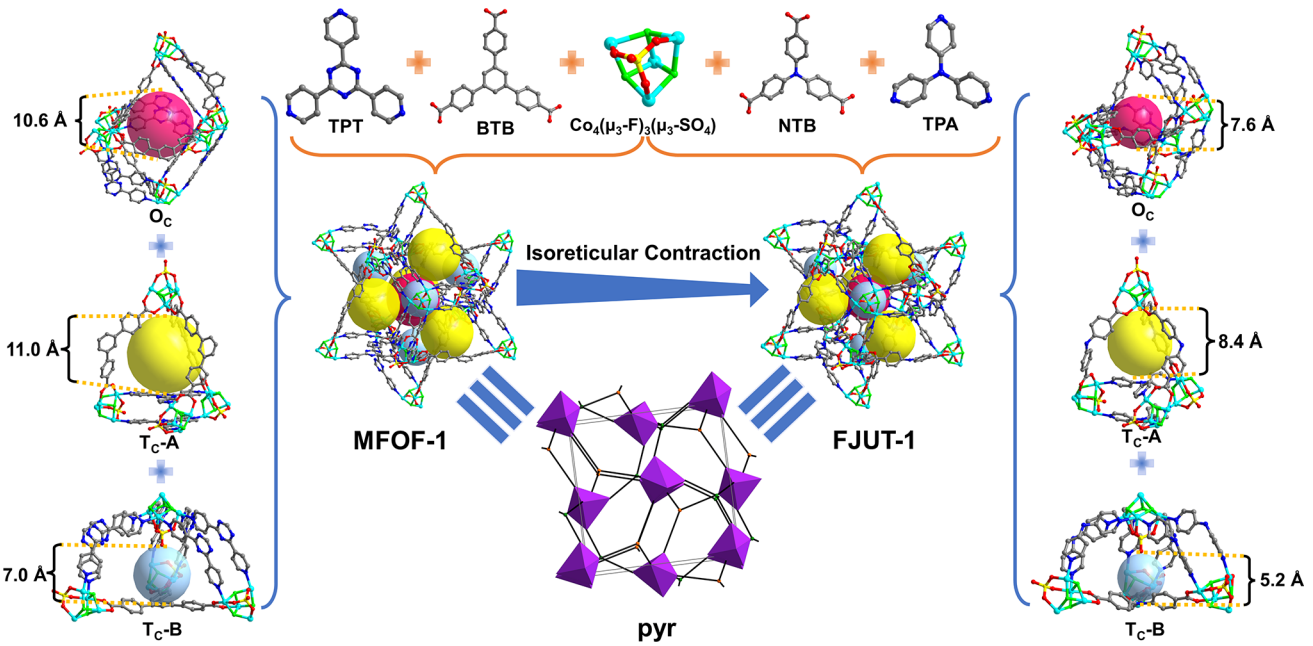

Figure 1. Schematic representation of the isoreticular contraction of MFOF-1 (left) and FJUT-1 (right) via decreasing the length of organic linkers. Atom color scheme: Co, turquoise; C, gray; N, blue; O, red; F, bright green; S, yellow. H atoms are omitted for clarity.

separation.[22−25] The pore system involving pore size/shape/volume and pore space environment can be precisely regulated by substituting the organic linkers with the same symmetry or the inorganic metal nodes based on the isostructural principle and building block strategy,[26−32] which in turn endows MOFs with enormous potentials for selective gas separation via the integration of pore size/shape matching and preferential binding interactions toward specific gas molecules.[33−36] So far, tremendous endeavors have been devoted to improving the enrichment and separation performance for specific gas molecules, in which the construction of cage-like mixed-ligands MOFs without open metal sites (OMSs), featuring small pore window size, functional pore space, and appropriate pore volume, has represented one of the most effective approaches.[37−43] For instance, the pore-space-partition-based MOFs (PSP-MOFs), with cage-like cavities, have shown high performance for gas adsorption and separation,[32,44−51] attributed to the relocation of the pore system, stemming from the introduction of the second spacers, involving compartmentalized small pore, functionalized pore space, and reserved appropriate pore volume. The segmented small pore size and functionalized pore surface impart enhanced gas separation through providing dramatically increased adsorbent−adsorbate binding sites toward specific gas molecules, while the preserved appropriate pore volume bestows PSP-MOFs with high gas adsorption performance, thereby making the PSP-MOFs a prominent scaffold for gas adsorption and separation, including C_2H_2 and CO_2 capture,[52,53] C_2H_2/CO_2,[54−56] C_2H_2/C_2H_4/C_2H_6,[57] and C_3H_6/C_3H_8 separation.[56,58,59] Additionally, the cage-like MOFs without OMSs usually exhibit relatively low adsorption enthalpy compared with the MOFs with OMSs, suggesting low energy demand for the regeneration of adsorbents. Nevertheless, to achieve simultaneously high capacity and separation selectivity for more challenging C_2H_2/CO_2 and C_2H_2/C_2H_4 separations, these cage-like MOFs usually suffer from unsatisfactory separation performance for C_2H_2/CO_2 and C_2H_2/C_2H_4 gas mixtures due to their similar physicochemical properties, despite showing good uptake capacities for C_2H_2, CO_2, and C_2H_4. Furthermore, it is still very difficult to achieve the fine-tuning of the pore size/shape/volume for cage-like MOFs via the isostructural principle especially for MOFs involving multiple linkers and unusual building blocks due to the significantly increased complexity for MOFs self-assembly arising from the diversity of coordination modes and unpredictable coordination directions of metal−organic coordination bonds.

The significant feature to boost the adsorbents' discrimination ability to C_2H_2 in C_2H_2/CO_2 and C_2H_2/C_2H_4 gas mixtures is to introduce suitable binding sites that can preferentially interact with C_2H_2 versus CO_2 and C_2H_4. Recently, fluorinated MOFs (fluorinated MOFs refer to MOFs containing fluorinated linkers, or fluoride anions, or fluoride-functionalized metal-clusters) have shown great potential for C_2H_2-separation-based applications, where the fluoride anions (F^-) can serve as hydrogen bond acceptors strongly interacting with C_2H_2 via C−H···F forces.[19,60−67] In this regard, we developed a fluoride- and sulfate-bridging Co_4-cluster-based mixed-ligand MOF, MFOF-1,[68] constructed from the tripodal carboxylic acid and pyridines ligands, as well as fluoride- and sulfate-bridged cubane-type tetranuclear cobalt clusters, in which the fluoride anions and sulfate (SO_4^{2-}) anions provide multiple potential binding sites for C_2H_2. Importantly, these two kinds of ligands are segregated in the defined position for engineering the coordination interspace involving pore size/shape/surface/volume, thereby paving the way for the design and construction of cage-like mixed-ligand MOFs for C_2H_2/CO_2 and C_2H_2/C_2H_4 separation.

In this work, a fluoride- and sulfate-bridging Co_4-cluster-based mixed-ligand MOF, FJUT-1 (FJUT stands for Fujian University of Technology) isostructural with MFOF-1 (Figure 1), featuring three types of polyhedral cages, has been successfully constructed from the contracted tripodal carboxylic acid and pyridine ligands [4,4′,4″-nitrilotribenzoic acid (NTB), and tri(pyridin-4-yl)amine (TPA)] (Figure S1), with the same cubane-type tetranuclear cobalt clusters ($[Co_4(\mu_3\text{-}F)_3(\mu_3\text{-}$

https://doi.org/10.1021/jacs.3c12032
J. Am. Chem. Soc. 2024, 146, 7341−7351

$SO_4)]^{3+}$), for C_2H_2 separation from C_2H_2/CO_2 and C_2H_2/C_2H_4 gas mixtures. FJUT-1 presents excellent chemical stability under harsh conditions, arising from the introduction of hydrophobic fluorinated $[Co_4(\mu_3\text{-}F)_3(\mu_3\text{-}SO_4)]^{3+}$ clusters. Remarkably, compared with the prototypical MFOF-1, FJUT-1 exhibits significantly increased C_2H_2 capture capacity, especially at low pressure (10 kPa), with the uptake reaching 2.5 times that of MFOF-1, together with enhanced selectivity for C_2H_2/CO_2 (1.7 times) and C_2H_2/C_2H_4 (3.0 times) than that of MFOF-1 at 10 kPa (vide infra). These superior results are due to the reduced cage cavity size, functionalized pore surface decorated with fluoride anions and sulfate anions, and appropriate pore volume. Furthermore, transient breakthrough experiments and theoretical calculations corroborate the result, in which the optimized pore nanospace and functionalized pore surface of F, O, and H atoms for C−H···F, C−H···O hydrogen bonds, and C≡C···H interactions play a critical collective role in this challenging C_2H_2/CO_2 and C_2H_2/C_2H_4 separation.

RESULTS AND DISCUSSION

Synthesis and Characterization of MOFs. The prototypical MFOF-1 was synthesized through the solvothermal reaction of 4,4′,4″-benzene-1,3,5-triyl-tribenzoate (BTB), 2,4,6-tri(4-pyridinyl)-1,3,5-triazine (TPT) and $CoSO_4{\cdot}7H_2O$ with tetrafluoroboric acid (HBF_4, 40 wt % in water) as the modulator in the mixed N,N-dimethylacetamide/methanol/1,4-dioxane (DMA/MeOH/Diox) solution at 120 °C for 5 days according to our reported method, featuring a cubane-type tetranuclear Co_4 cluster ($[Co_4(\mu_3\text{-}F)_3(\mu_3\text{-}SO_4)]^{3+}$), and three kinds of polyhedral cages, one octahedral cage (O_c), and two tetrahedral cages (T_c-A and T_c-B), with the cavity diameters of 10.6, 11.0, and 7.0 Å, respectively. The tetranuclear Co_4 cluster bearing fluoride anions and sulfate anions impart MFOF-1 with preferential C_2H_2 adsorption through potential multiple adsorbent−adsorbate binding interactions, while the polyhedral cages with high pore volume endow MFOF-1 with high gas adsorption capacity. By substitution of the organic BTB and TPT linkers with the contracted NTB and TPA linkers, a novel fluorinated MOF, FJUT-1, with the same *pyr* topology network, was afforded through the solvothermal reaction. Single-crystal X-ray diffraction reveals that FJUT-1 crystallizes in cubic space group $P2_13$ (Table S2). There is one crystallographically independent Co^{II} ion, one-third of another independent Co^{II} ion, one-third of a deprotonated NTB^{3-} ligand, one-third of two independent TPA ligands, half of one sulfate anion, and one μ_3-F^- anion in the asymmetric unit (Figure S3). Four Co^{II} ions are connected by three μ_3-F^- anions and one μ_3-SO_4^{2-} anion, forming the cubic Co_4 cluster with two types of Co^{II} ions (Co1 and Co2). The Co^{II} ions adopt a distorted octahedral coordination geometry, where Co1 is connected by three μ_3-F^- anions, and three carboxylic oxygen atoms from different NTB ligands, while Co2 is coordinated by one oxygen from one sulfate anion, one carboxylic oxygen atom from NTB ligand, two nitrogen atoms from two independent TPA ligands, and two μ_3-F^- anions (Figure S4). The Co_4 cluster is connected by three NTB ligands and six TPA ligands, while NTB and TPA ligands are connected by three Co_4 clusters, thus forming a 3D *pyr* topology network. Similarly, FJUT-1 contains three types of polyhedral cages decorated with F^- and SO_4^{2-} anions, one octahedral cage (O_c), and two tetrahedral cages (T_c-A and T_c-B) (Figure 1). It is worth noting that the cage cavity diameters in FJUT-1 are effectively reduced from 10.6 to 7.6 Å for cage O_c, 11.0 to 8.4 Å for cage T_c-A, and 7.0 to 5.2 Å for T_c-B, respectively, in comparison with the prototypical MFOF-1, which presents the potential for reinforcing the binding affinity toward C_2H_2 through multiple supramolecular interactions, as confirmed by the experiments and molecular modeling (vide infra) (Figure S6).

Phase Purity, Stability, and Porosity Description. The scanning electron microscope (SEM) images were carried out to demonstrate the octahedral morphology of FJUT-1 (Figure S13). The energy-dispersive X-ray spectroscopy (EDS) mapping images reveal that the C, N, O, S, F, and Co elements are uniformly distributed throughout the samples of FJUT-1 (Figure S14). Powder X-ray diffraction (PXRD) patterns were conducted to affirm the phase purity of bulky MFOF-1 and FJUT-1 samples (Figures S19 and S20). The thermogravimetric analysis (TGA) was performed to assess the thermal stability of FJUT-1, manifesting that FJUT-1 can be stable up to 380 °C (Figure S23). The permanent porosity of MFOF-1 and FJUT-1 have been confirmed by N_2 adsorption isotherms at 77 K, revealing both the typical type-I adsorption behavior of microporous materials (Figure 2a). The saturated adsorption capacity of FJUT-1 is 315.1 $cm^3\ g^{-1}$, which is lower than that of MFOF-1 (600 $cm^3\ g^{-1}$) as a consequence of the contracted cage sizes of FJUT-1. The BET surface areas for MFOF-1 and FJUT-1 are 2287 and 1240 $m^2\ g^{-1}$, respectively (Figures S25 and S26), corresponding to total pore volumes of 0.93 and 0.49 $cm^3\ g^{-1}$, respectively (Table S3). The pore size distributions by using the density functional theory (DFT) method are estimated to be centered at 5.8 and 6.9 Å, smaller than those of MFOF-1 (7.2 and 10.3 Å, respectively), agreeing very well with the calculated values from the crystal structures. In our previous work, the introduction of fluoride- and sulfate-bridged Co_4 clusters into MFOF-1 has been verified to significantly improve the skeleton structure resistant to harsh acid/base corrosion. Therefore, the isostructural FJUT-1 with smaller cage cavity sizes might present higher chemical stability. To verify the hypothesis, PXRD patterns and SEM images were performed to reveal that FJUT-1 maintains good crystallinity and structure integrity after the samples were soaked in an aqueous solution with different pH values (pH = 1−13) (Figures 2b and S18), whereas the prototypical MFOF-1 loses its crystallinity and intact structural morphology in the aqueous solution with pH = 13 (Figures S17 and S21). In addition, the N_2 adsorption isotherms of FJUT-1 samples treated with pH = 2 and 12 aqueous solutions further prove the excellent chemical stability of FJUT-1 (Figure 2c). Notably, the pore space of FJUT-1 has been finely tuned through the reticular chemistry approach by comparison with MFOF-1, in which the cage sizes are effectively reduced, the pore surface is precisely modified, and the appropriate pore volume is preserved, thus giving rise to great potential for selective C_2H_2 separation from CO_2 and C_2H_4 through a significantly enhanced confinement effect.

Single-Component Adsorption Measurements. To examine the gas adsorption and separation performance, the optimum activation temperature of FJUT-1 was found to be 120 °C for 12 h, which was confirmed by TGA and the weight time curves (Figures S23 and S24). Subsequently, C_2H_2, CO_2, C_2H_4, and CH_4 adsorption experiments were conducted at 273, 298, and 313 K (Figures 3a and S27−S44), respectively. As shown in Figure 3a, both MFOF-1 and FJUT-1 exhibit much higher C_2H_2 uptake (105.9 $cm^3\ g^{-1}$ for MFOF-1, and 133.2 $cm^3\ g^{-1}$ for FJUT-1) than CO_2 (51.5 $cm^3\ g^{-1}$ for MFOF-1, and 108.4 $cm^3\ g^{-1}$ for FJUT-1), C_2H_4 (77.7 $cm^3\ g^{-1}$ for MFOF-1, and 106.5 $cm^3\ g^{-1}$ for FJUT-1), and CH_4 (11.3 $cm^3\ g^{-1}$ for MFOF-1, and 23.0 $cm^3\ g^{-1}$ for FJUT-1) at 298 K and 100 kPa, which suggest

https://doi.org/10.1021/jacs.3c12032
J. Am. Chem. Soc. 2024, 146, 7341−7351

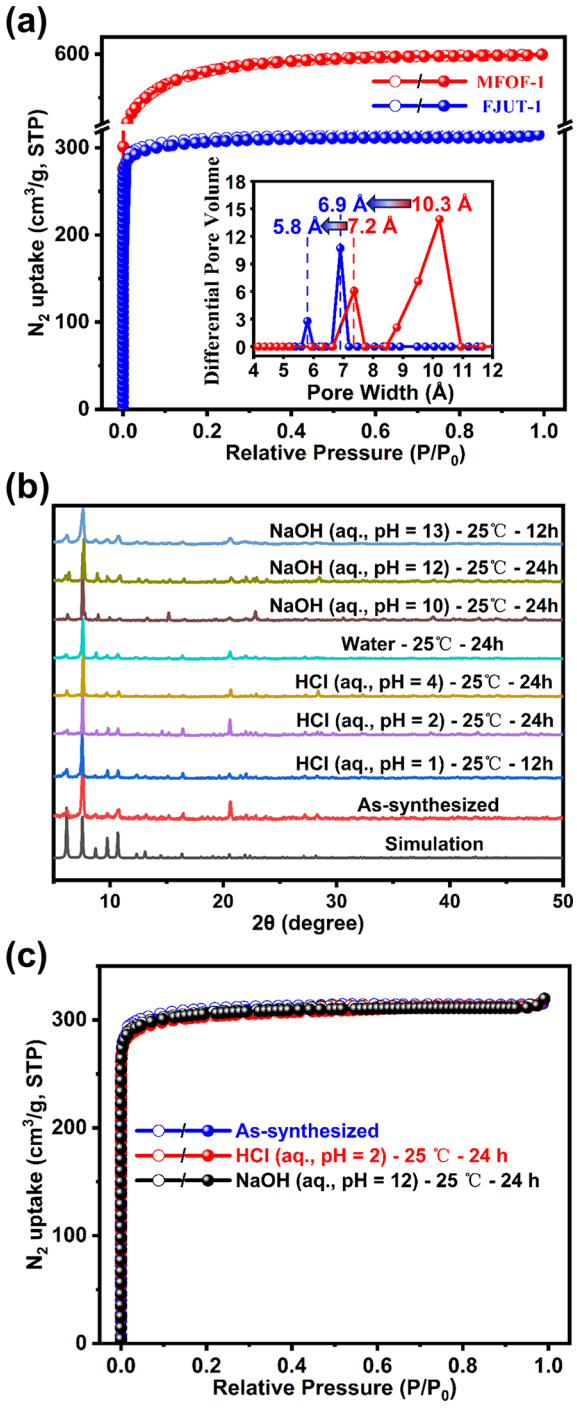

Figure 2. Stability and porosity of FJUT-1. (a) N_2 adsorption isotherms at 77 K and (inset) corresponding DFT pore size analyses of MFOF-1 (red line) and FJUT-1 (blue line). (b) PXRD patterns for FJUT-1 after treatment under different conditions. (c) N_2 adsorption isotherms at 77 K for FJUT-1 obtained under different conditions, suggesting its high chemical stability.

that both MOFs are capable of selectively adsorbing C_2H_2 over CO_2, C_2H_4, and CH_4. However, in comparison with the prototypical MFOF-1, FJUT-1 showed significantly improved adsorption capacities for C_2H_2, CO_2, C_2H_4, and CH_4 at 298 K, especially at partial low pressure (10 kPa) reaching more than a 2.5-fold excess of MFOF-1 (Figure 3b–d). Since the industrially produced C_2H_2 and C_2H_4 usually contain a small amount of CO_2 and C_2H_2, the gas separation performance is closely related to the gas adsorption behavior in the low-pressure range, and thus the larger difference in the uptake capacity of either C_2H_2/CO_2 or C_2H_2/C_2H_4 in low partial pressure can give rise to more superior separation performance.[69,70] The difference in uptakes of either C_2H_2/CO_2 (30.72 $cm^3\ g^{-1}$) or C_2H_2/C_2H_4 (24.70 $cm^3\ g^{-1}$) on FJUT-1 at low pressure (10 kPa) is much higher than those of MFOF-1 (17.71 $cm^3\ g^{-1}$ for C_2H_2/CO_2, and 15.08 $cm^3\ g^{-1}$ for C_2H_2/C_2H_4), suggesting enhanced C_2H_2 separation potential from C_2H_2/CO_2 and C_2H_2/C_2H_4 gas mixture. Noteworthily, the incorporation of OMSs into MOFs is an efficient strategy for improving the C_2H_2 capture capacity via C≡C···M (M = metal ions) interactions. However, FJUT-1 (133.2 $cm^3\ g^{-1}$) without OMSs possesses much better C_2H_2 adsorption performance than many reported MOFs with OMSs at 298 K and 100 kPa (Tables S4 and S5), such as, NKMOF-1-Ni (61.0 $cm^3\ g^{-1}$),[69] ZJU-74 (85.7 $cm^3\ g^{-1}$),[71] JNU-2 (103.0 $cm^3\ g^{-1}$),[72] UTSA-74 (108.05 $cm^3\ g^{-1}$),[73] ATC-Cu (112.2 $cm^3\ g^{-1}$),[74] Zn-MOF-74 (123.05 $cm^3\ g^{-1}$),[73] and LIFM-26 (Fe[II]/Fe[III]) (131.0 $cm^3\ g^{-1}$),[75] especially at 10 kPa and 298 K, presenting the C_2H_2 adsorption of 62.76 $cm^3\ g^{-1}$, just lower than the benchmark HKUST-1 (73.78 $cm^3\ g^{-1}$),[42] FeNi-M'MOF (74.91 $cm^3\ g^{-1}$),[75] ATC-Cu (85.79 $cm^3\ g^{-1}$),[74] and ZJU-50 (86.34 $cm^3\ g^{-1}$) (Table S5).[42] Moreover, the repeated C_2H_2, CO_2, and C_2H_4 adsorption isotherms affirm the excellent recyclability of FJUT-1 (Figures S53–S55). From the above results, it can be concluded that the substitutions of BTB and TPT linkers with the contractive NTB and TPA linkers effectively reduce the cage size yet preserve suitable pore volume, while the preserved functional Co_4 clusters bearing F^- and SO_4^{2-} anions endow the cage space with polar environments, collaboratively posing a significant enhancement in C_2H_2/CO_2 and C_2H_2/C_2H_4 separation processes.

The isosteric heat of adsorption (Q_{st}) for C_2H_2, CO_2, and C_2H_4 on MFOF-1 and FJUT-1 was calculated using the Clausius–Clapeyron equation on the basis of the adsorption isotherms at 273, 298, and 313 K. As depicted in Figure 3e,f, both MFOF-1 and FJUT-1 show much higher C_2H_2 Q_{st} values than CO_2 and C_2H_4, which manifests that both MOFs possess C_2H_2/CO_2 and C_2H_2/C_2H_4 separation potential to some extent. By comparison with the prototypical MFOF-1 (31.88 kJ mol^{-1} for C_2H_2, 25.97 kJ mol^{-1} for CO_2, and 21.53 kJ mol^{-1} for C_2H_4, respectively), FJUT-1 exhibits higher C_2H_2 (43.75 kJ mol^{-1}), CO_2 (37.39 kJ mol^{-1}), and C_2H_4 (31.01 kJ mol^{-1}) Q_{st} values at near-zero coverage, suggesting the enhanced adsorbent–adsorbate interactions ascribed to the contraction of the cage cavity sizes. In addition, the difference in the Q_{st} values (ΔQ_{st}) represents the binding selectivity of adsorbents; the ΔQ_{st} of C_2H_2/CO_2 (6.36) and C_2H_2/C_2H_4 (12.74) on FJUT-1 is also higher than those of MFOF-1 (5.91 for C_2H_2/CO_2, and 10.35 for C_2H_2/C_2H_4) (Table S3), indicative of improved C_2H_2/CO_2 and C_2H_2/C_2H_4 separation performance, further affirming the effectiveness of the cage cavity sizes reduction. It is worth noting that the C_2H_2 Q_{st} value of FJUT-1 is much lower than many reported MOFs with OMSs, such as NKMOF-1-Ni (60.3 kJ mol^{-1}),[69] ZJU-74 (45–65 kJ mol^{-1}),[71] Cu^I@UiO-66-$(COOH)_2$ (74.5 kJ mol^{-1}),[77] ATC-Cu (79.1 kJ mol^{-1}),[74] etc., indicative of sufficient adsorption–desorption reversibility of FJUT-1 (Table S4).

In order to evaluate the adsorptive separation performance of MFOF-1 and FJUT-1, the selectivity of C_2H_2/CO_2 (50:50, v:v) and C_2H_2/C_2H_4 (1:99, v:v) was calculated by using ideal adsorbed solution theory (IAST). As depicted in Figure 3g,h, both MOFs present good C_2H_2/CO_2 (3.66 for MFOF-1, and

https://doi.org/10.1021/jacs.3c12032
J. Am. Chem. Soc. 2024, 146, 7341–7351

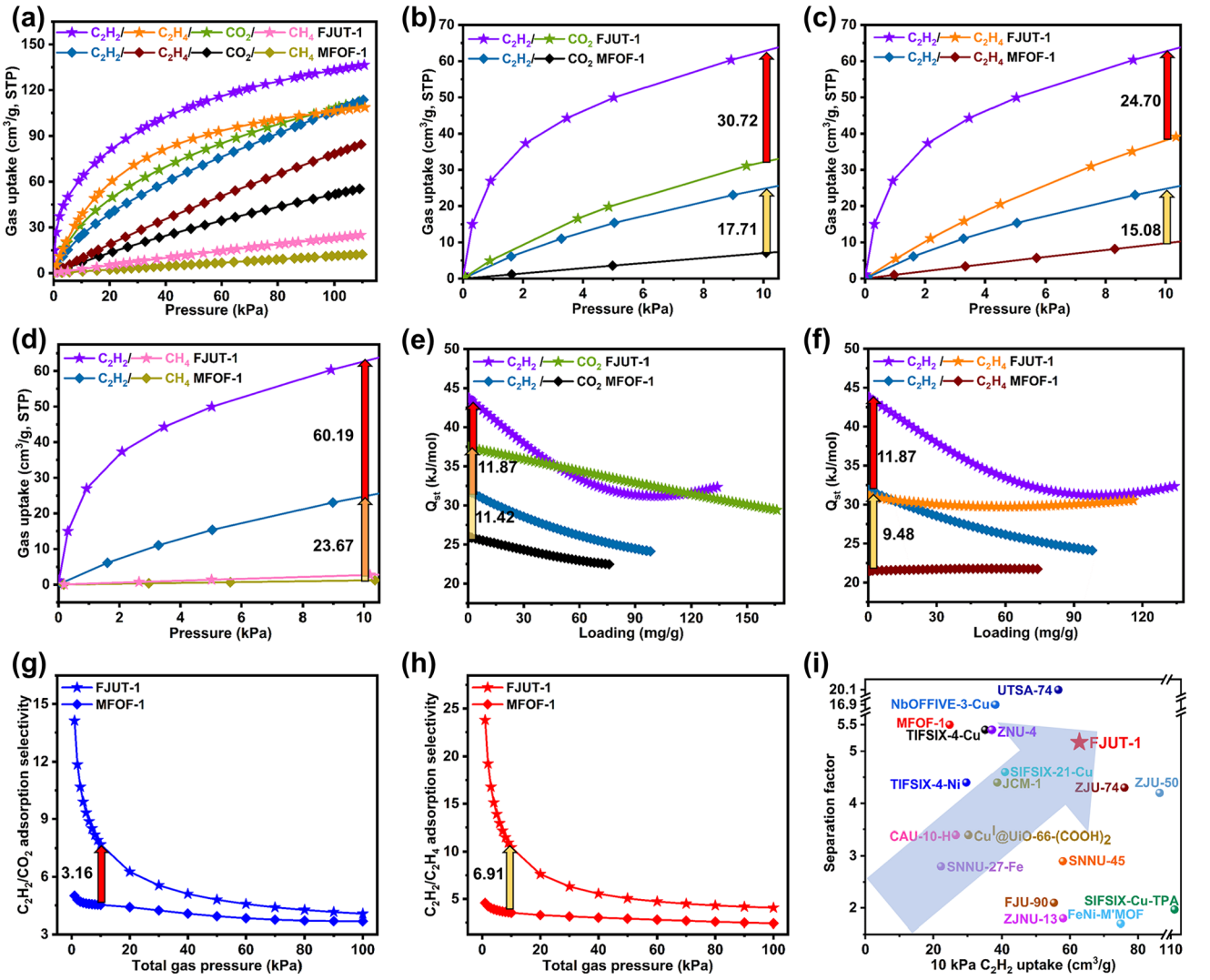

Figure 3. Gas adsorption performance for MFOF-1 and FJUT-1. (a) Experimental adsorption isotherms of C_2H_2, C_2H_4, CO_2, and CH_4 for MFOF-1 and FJUT-1 at 298 K, respectively. Comparison of (b) C_2H_2 and CO_2, (c) C_2H_2 and C_2H_4, and (d) C_2H_2 and CH_4 adsorption isotherms of MFOF-1 and FJUT-1 in the region of 0−10 kPa at 298 K. Comparison of isosteric heats (Q_{st}) of (e) C_2H_2 and CO_2, (f) C_2H_2 and C_2H_4 for MFOF-1 and FJUT-1. (g) IAST selectivities of MFOF-1 and FJUT-1 for C_2H_2/CO_2 (50:50, v:v) at 298 K. (h) IAST selectivities of MFOF-1 and FJUT-1 for C_2H_2/C_2H_4 (1:99, v:v) at 298 K. (i) Comparison of the C_2H_2/CO_2 (50:50, v:v) separation factor and C_2H_2 uptake for the best-performing MOF materials at 10 kPa under ambient conditions.

4.06 for FJUT-1) and C_2H_2/C_2H_4 (2.42 for MFOF-1, and 4.07 for FJUT-1) selectivity at 298 K and 100 kPa, indicating good selective C_2H_2 separation from CO_2 and C_2H_4. However, FJUT-1 presents higher selectivity for both C_2H_2/CO_2 and C_2H_2/C_2H_4 than MFOF-1 (4.53 and 3.54 at 298 K and 10 kPa), especially in low-pressure coverage, with the values of 7.69 and 10.45 at 298 K and 10 kPa, implying improved C_2H_2/CO_2 and C_2H_2/C_2H_4 separation performance, which can be ascribed to the stronger confinement effect toward C_2H_2 in FJUT-1 as a consequence of the contracted cage cavity size. The C_2H_2/CO_2 selectivity for FJUT-1 is comparable with some previously reported MOFs, such as UiO-66-$(COOH)_2$ (2.1),[77] SNNU-29-Mn (2.9),[55] UPC-200(Al)-F-BIM (3.15),[38] and Cu-CPAH (3.6) (Table S4).[78]

Breakthrough Experiment. To further examine the practical separation potential of MFOF-1 and FJUT-1, the dynamic breakthrough experiments were carried out through a stainless-steel column at 298, 308, and 318 K, under 100 kPa, where C_2H_2/CO_2 (50:50, v:v) or C_2H_2/C_2H_4(1:99, v:v) gas mixtures flowed over the fixed-bed filled with tightly packed MOFs samples at a rate of 2, 5, and 10 mL min^{-1} (Figures 4 and 5). For C_2H_2/CO_2 or C_2H_2/C_2H_4, both MOFs showcase excellent C_2H_2 separation performance from C_2H_2/CO_2 or C_2H_2/C_2H_4 gas mixtures, in which CO_2 or C_2H_4 first elutes out from the packed column and quickly reaches saturation without detectable C_2H_2, whereas C_2H_2 retains in the packed column with a remarkable long time until it is saturated in the frameworks. Remarkably, FJUT-1 presents much longer C_2H_2 breakthrough time than MFOF-1 for both C_2H_2/CO_2 and C_2H_2/C_2H_4 gas mixtures, implying the significantly improved C_2H_2 separation performance attributed to the enhanced C_2H_2-framework interactions and reserved appropriate pore volume in FJUT-1.

For C_2H_2/CO_2 (50:50, v:v), the breakthrough interval of FJUT-1 between C_2H_2 and CO_2 is 31.7 min g^{-1} and the C_2H_2 capture capacity is estimated to be 4.83 mmol g^{-1} based on a single breakthrough curve with a flow rate of 2 mL min^{-1} at 298 K and 100 kPa (Figures 4a and S97), which is comparable with

https://doi.org/10.1021/jacs.3c12032
J. Am. Chem. Soc. 2024, 146, 7341−7351

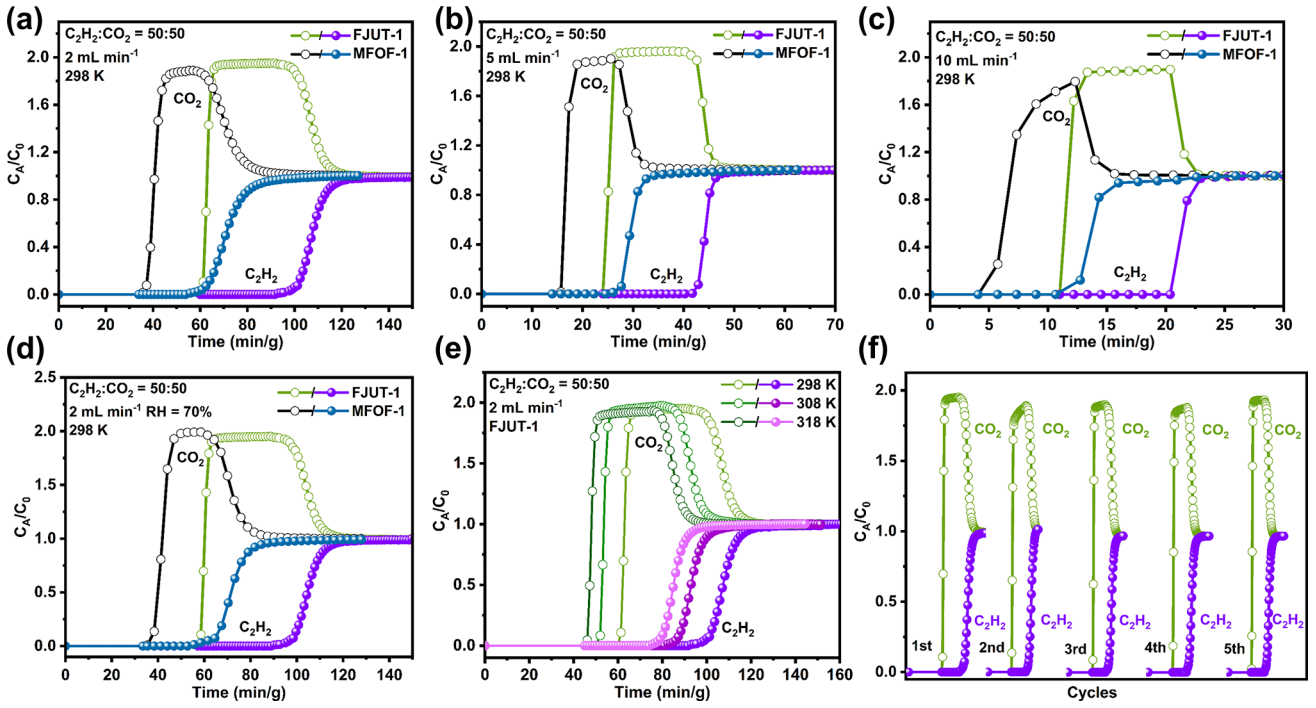

Figure 4. Experimental breakthrough curves for C_2H_2/CO_2 (50:50, v:v) gas mixtures of MFOF-1 and FJUT-1 at 100 kPa. Breakthrough curves for MFOF-1 and FJUT-1 at 298 K with a total flow of (a) 2 mL min^{-1}, (b) 5 mL min^{-1}, and (c) 10 mL min^{-1}, respectively. (d) Breakthrough curves for MFOF-1 and FJUT-1 with a total flow of 2 mL min^{-1} at 298 K under 70% humidity. (e) Breakthrough curves of FJUT-1 with a total flow of 2 mL min^{-1} at various temperatures. (f) Recyclability of FJUT-1 under multiple breakthrough tests with a total flow of 2 mL min^{-1} at 298 K.

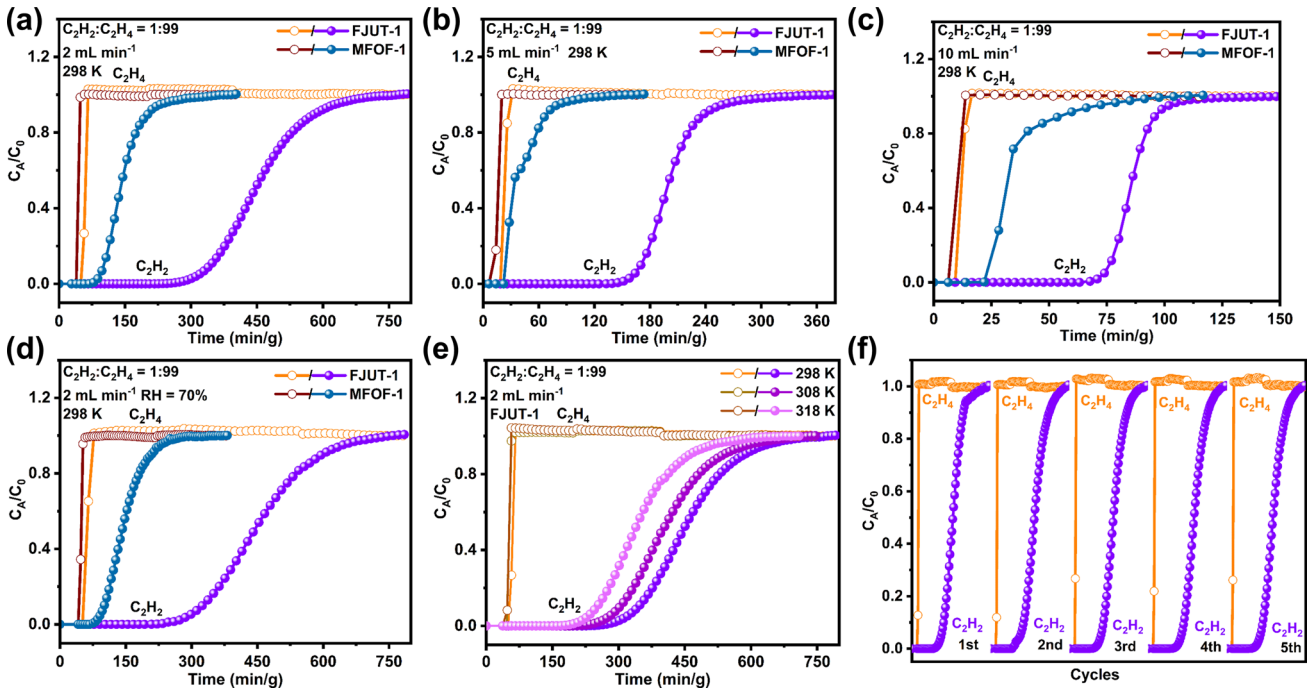

Figure 5. Experimental breakthrough curves for C_2H_2/C_2H_4 (1:99, v:v) gas mixtures of MFOF-1 and FJUT-1 at 100 kPa. Breakthrough curves for MFOF-1 and FJUT-1 at 298 K with a total flow of (a) 2 mL min^{-1}, (b) 5 mL min^{-1}, and (c) 10 mL min^{-1}, respectively. (d) Breakthrough curves for MFOF-1 and FJUT-1 with a total flow of 2 mL min^{-1} at 298 K under 70% humidity. (e) Breakthrough curves of FJUT-1 with a total flow of 2 mL min^{-1} at various temperatures. (f) The recyclability of FJUT-1 under multiple breakthrough tests with a total flow of 2 mL min^{-1} at 298 K.

the benchmark MOFs like FJU-90 (22 min g^{-1}, 1.87 mmol g^{-1}),[54] JNU-1 (34 min g^{-1}, 2.84 mmol g^{-1}),[79] ZJU-74 (36 min g^{-1}, 3.64 mmol g^{-1}),[71] and SNNU-98-Mn (39 min g^{-1}, 4.9 mmol g^{-1}).[12] The productivity of C_2H_2 (≥99.5%) is calculated to be 2.12 mmol g^{-1} based on desorption of the gas-saturated FJUT-1 (Figure S95). It is worth mentioning that the separation factor is another important criterion for evaluating the separation potential of the MOFs. The C_2H_2/CO_2 (50:50, v:v) separation factor for FJUT-1 is calculated to be 5.17 based on a single breakthrough experiment under a flow rate of 2 mL

https://doi.org/10.1021/jacs.3c12032
J. Am. Chem. Soc. 2024, 146, 7341−7351

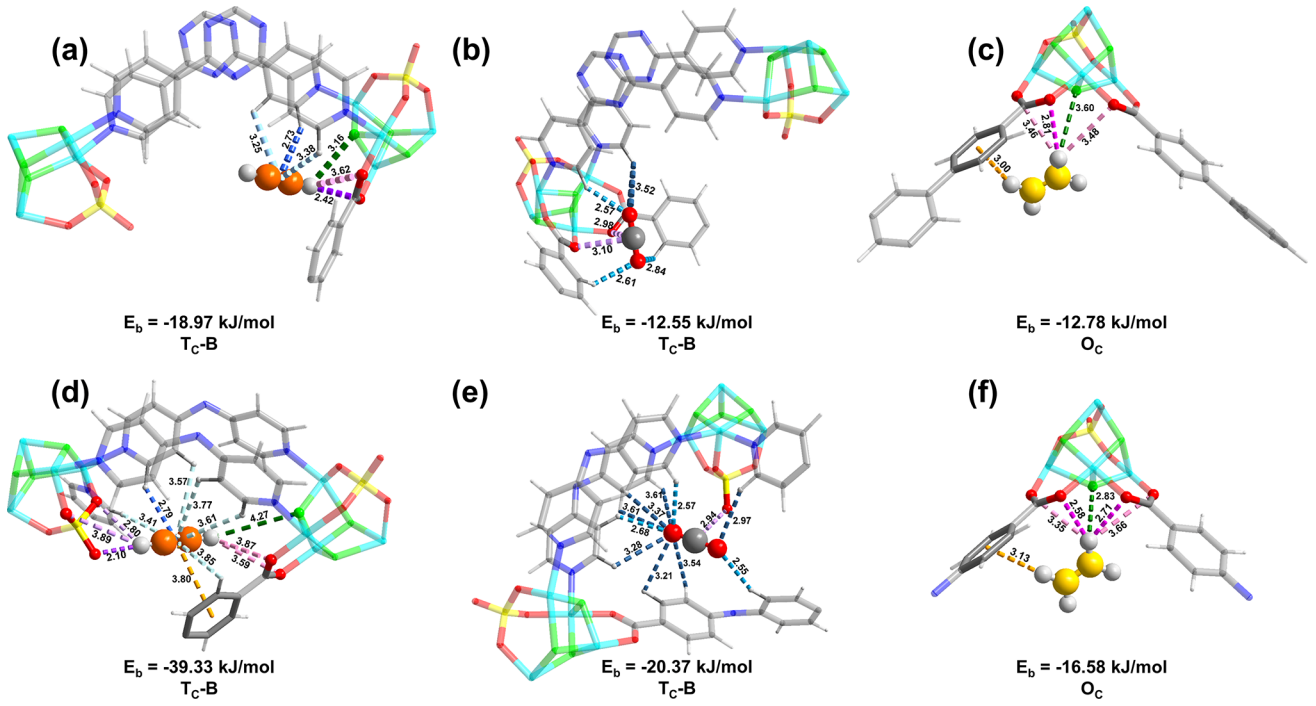

Figure 6. DFT calculated preferential adsorption sites and binding energies of (a) C_2H_2, (b) CO_2, and (c) C_2H_4 in MFOF-1 and (d) C_2H_2, (e) CO_2, and (f) C_2H_4 in FJUT-1, respectively.

min^{-1}, which is much higher than many top-performing MOFs, including SIFSIX-21-Cu (4.6),[28] ZJU-74 (4.3),[71] ZJU-50 (4.2),[42] CAU-10-H (3.4),[80] SNNU-45 (2.9),[8] FJU-90 (2.1),[54] SIFSIX-Cu-TPA (1.97),[40] FeNi-M'MOF (1.7),[76] and lower than the benchmark NbOFFIVE-3-Cu (16.9)[28] and UTSA-74 (20.1)[73] (Figure 3i, Table S6). For C_2H_2/C_2H_4 (1:99, v:v), C_2H_4 gas broke through the packed column at 57.1 min g^{-1}, while C_2H_2 gas was trapped and eluted until 217 min g^{-1}, corresponding to the breakthrough interval of 159.9 min g^{-1} on the basis of a single breakthrough curve with a flow rate of 2 mL min^{-1} at 298 K and 100 kPa (Figure 5a). The calculated C_2H_2 capture capacity is 0.41 mmol g^{-1} based on the single breakthrough isotherm with a flow rate of 2 mL min^{-1} at 298 K and 100 kPa. The calculated C_2H_4 productivity with ≥99.9% purity is estimated to be 13.94 mmol g^{-1} based on one breakthrough adsorption curve (Figure S96).

To evaluate the C_2H_2 separation performance from C_2H_2/CO_2 and C_2H_2/C_2H_4 on MFOF-1 and FJUT-1 under humidity conditions, dynamic breakthrough experiments under 70% humidity were implemented, which shows that FJUT-1 possesses much better C_2H_2 separation performance than the prototypical MFOF-1 (Figures 4d,5d, S98, S99, S103 and S104). The dynamic breakthrough experiments on FJUT-1 samples after treatment by aqueous solutions with pH = 2, and 12, were performed at a flow rate of 2 mL min^{-1} at 298 K and 100 kPa, which presents good C_2H_2/CO_2 and C_2H_2/C_2H_4 separation, suggesting its robustness (Figures S98 and S102). Moreover, the consecutive dynamic breakthrough experiments for C_2H_2/CO_2 and C_2H_2/C_2H_4 on FJUT-1 were performed with a flow rate of 2 mL min^{-1} at 298 K and 100 kPa (Figures 4f, 5f, S101, S102, S106, and S107), which demonstrates its outstanding recyclability and durability, further confirmed by the PXRD patterns (Figures S19 and S20).

DFT-D Modeling of Binding Sites. To probe the distinct adsorption mechanism, dispersion-corrected DFT simulations were implemented. As shown in Figures 6 and S109−S111, for both MFOF-1 and FJUT-1, C_2H_2 and CO_2 are preferentially located in the tetrahedral T_c-B cage, whereas C_2H_4 and CH_4 are mainly situated in the O_c cage. For MFOF-1, C_2H_2 is located in the T_c-B cage surrounded by one Co_4 cluster, two TPT linkers, and one BTB linker, in which the C−H···O (2.42 and 3.62 Å), C−H···F (3.16 Å), and C≡C···H (2.73, 3.25, and 3.38 Å) interactions happen. For comparison, CO_2 is fixed in the T_c-B cage comprised of one Co_4 cluster, two TPT linkers, and two BTB linkers through C−O···H (2.57, 2.61, 2.84, and 3.52 Å) and C═C···O (2.98 and 3.10 Å) interactions. C_2H_4 is banded in the O_c cage composed of two BTB linkers and one Co_4 cluster via C−H···O (2.81, 3.46, and 3.48 Å), C−H···F (3.60 Å), and C−H···π (3.00 Å) interactions. For FJUT-1, C_2H_2 is located in the similar T_c-B cage as that in MFOF-1, yet with stronger C_2H_2-binding interaction through forming a C_2H_2-nanotrap surrounded by two Co_4 clusters, one NTB linker, and three TPA linkers, in which C_2H_2 interacts with the framework through C−H···O (2.10, 2.80, 3.59, 3.87, and 3.89 Å), C−H···F (4.27 Å), C≡C···π (3.80 Å), and C≡C···H (2.79, 3.41, 3.57, 3.61, 3.77, and 3.85 Å). In comparison, CO_2 interacts with the framework mainly through C−O···H (2.55, 2.57, 2.68, 2.97, 3.21, 3.28, 3.37, 3.54, 3.61, and 3.61 Å) and C═C···O (2.94 Å) interactions. C_2H_4 is located in the O_c cage surrounded by one Co_4 cluster and two NTB linkers, in which C−H···O (2.58, 2.71, 3.35, and 3.66 Å), C−H···F (2.83 Å), and C−H···π (3.13 Å) interactions occur. The calculated C_2H_2, CO_2, and C_2H_4 binding energies for FJUT-1 are 39.33, 20.37, and 16.58 kJ mol^{-1}, which are higher than those of MFOF-1 (18.97, 12.55, and 12.78 kJ mol^{-1}, respectively), unveiling the enhanced gas-framework interactions and optimized C_2H_2 separation in FJUT-1 due to the contracted cage cavity size. Overall, the contraction of the cage cavity size and the reservation of electronegative F^- and SO_4^{2-} anions collaboratively lead to the significantly improved C_2H_2

https://doi.org/10.1021/jacs.3c12032
J. Am. Chem. Soc. 2024, 146, 7341−7351

separation performance from C_2H_2/CO_2 and C_2H_2/C_2H_4 gas mixtures.

CONCLUSIONS

In summary, we have successfully synthesized a fluoride- and sulfate-bridging Co_4-cluster-based mixed-ligand MOF with three kinds of polyhedral cages, FJUT-1, by substituting the BTB and TPT ligands with the contracted NTB and TPA ligands in the prototypical MFOF-1 based on the reticular chemistry strategy. FJUT-1 presents excellent thermal and chemical stability due to the incorporation of the hydrophobic fluoride- and sulfate-bridging Co_4 clusters. Significantly, FJUT-1, isostructural with MFOF-1, shows greatly improved C_2H_2 capture capacity, and selective C_2H_2 separation performance due to the reduced cage cavity size, polar pore surface decorated with electronegative F^- and SO_4^{2-} anions, and appropriate pore volume, which is well corroborated by the dynamic breakthrough experiments under three different temperatures and 70% humidity. Molecular modeling studies reveal that FJUT-1 has enhanced binding affinity toward C_2H_2 than MFOF-1 owing to the enhanced confinement effect through stronger collective interactions involving C−H···O, C−H···F, and other van der Waals. This work may open up a new avenue for the future rational design and construction of cage-like mixed-ligand MOFs with customized pore nanospace for C_2H_2 separation-related applications.

ASSOCIATED CONTENT

Supporting Information

The Supporting Information is available free of charge at https://pubs.acs.org/doi/10.1021/jacs.3c12032.

SEM, EDS, TGA, and additional characterization data (PDF)

Accession Codes

CCDC 2287568 contains the supplementary crystallographic data for this paper. These data can be obtained free of charge via www.ccdc.cam.ac.uk/data_request/cif, or by emailing data_request@ccdc.cam.ac.uk, or by contacting The Cambridge Crystallographic Data Centre, 12 Union Road, Cambridge CB2 1EZ, UK; fax: + 44 1223 336033.

AUTHOR INFORMATION

Corresponding Authors

Lei Zhang − *Collaborative Innovation Center for Intelligent and Green Mold and Die of Fujian Province, College of Materials Science and Engineering, Fujian University of Technology, Fuzhou, Fujian 350118, China;* orcid.org/0000-0001-6901-4038; Email: leizhang@fjut.edu.cn

Cheng-Xia Chen − *MOE Laboratory of Bioinorganic and Synthetic Chemistry, Lehn Institute of Functional Materials, School of Chemistry, Sun Yat-Sen University, Guangzhou 510006, China*; Email: chenchx29@mail.sysu.edu.cn

Shengqian Ma − *Department of Chemistry, University of North Texas, Denton, Texas 76201, United States;* orcid.org/0000-0002-1897-7069; Email: Shengqian.Ma@unt.edu

Authors

Taotao Xiao − *Collaborative Innovation Center for Intelligent and Green Mold and Die of Fujian Province, College of Materials Science and Engineering, Fujian University of Technology, Fuzhou, Fujian 350118, China*

Xiayun Zeng − *Collaborative Innovation Center for Intelligent and Green Mold and Die of Fujian Province, College of Materials Science and Engineering, Fujian University of Technology, Fuzhou, Fujian 350118, China*

Jianjun You − *Collaborative Innovation Center for Intelligent and Green Mold and Die of Fujian Province, College of Materials Science and Engineering, Fujian University of Technology, Fuzhou, Fujian 350118, China*

Ziyu He − *Collaborative Innovation Center for Intelligent and Green Mold and Die of Fujian Province, College of Materials Science and Engineering, Fujian University of Technology, Fuzhou, Fujian 350118, China*

Qianting Wang − *Collaborative Innovation Center for Intelligent and Green Mold and Die of Fujian Province, College of Materials Science and Engineering, Fujian University of Technology, Fuzhou, Fujian 350118, China*

Ayman Nafady − *Department of Chemistry, College of Science, King Saud University, Riyadh 11451, Saudi Arabia*

Abdullah M. Al-Enizi − *Department of Chemistry, College of Science, King Saud University, Riyadh 11451, Saudi Arabia;* orcid.org/0000-0002-3967-5553

Complete contact information is available at: https://pubs.acs.org/10.1021/jacs.3c12032

Notes

The authors declare no competing financial interest.

ACKNOWLEDGMENTS

This work was supported by the National Natural Science Foundation of China (21701024 and 22001271), the Natural Science Foundation of Fujian Province of China (2022J01944, 2022T3066, and 2021T3046), the Foundation for Distinguished Young Talents in Higher Education of Fujian Province (GY-Z17067), the Scientific Research Foundation of Fujian University of Technology (GY-Z17001 and GY-Z18175). Partial support from the Robert A. Welch Foundation (B-0027) and Researchers Supporting Program (RSP2024R79) at King Saud University, Riyadh, Saudi Arabia is also acknowledged.

REFERENCES

(1) Schobert, H. Production of acetylene and acetylene-based chemicals from coal. *Chem. Rev.* **2014**, *114*, 1743−1760.

(2) Trotuş, I. T.; Zimmermann, T.; Schüth, F. Catalytic reactions of acetylene: a feedstock for the chemical industry revisited. *Chem. Rev.* **2014**, *114*, 1761−1782.

(3) Ren, T.; Patel, M.; Blok, K. Olefins from conventional and heavy feedstocks: Energy use in steam cracking and alternative processes. *Energy* **2006**, *31*, 425−451.

(4) Chai, Y. C.; Han, X.; Li, W. Y.; Liu, S. S.; Yao, S. K.; Wang, C.; Shi, W.; Da-Silva, I.; Manuel, P.; Cheng, Y. Q.; Daemen, L. D.; Ramirez-Cuesta, A. J.; Tang, C. C.; Jiang, L.; Yang, S. H.; Guan, N. J.; Li, L. D. Control of zeolite pore interior for chemoselective alkyne/olefin separations. *Science* **2020**, *368*, 1002−1006.

(5) Cui, W. G.; Hu, T. L.; Bu, X. H. Metal-organic framework materials for the separationand and purification of light hydrocarbons. *Adv. Mater.* **2020**, *32*, No. 1806445.

(6) Yang, L. F.; Qian, S. H.; Wang, X. B.; Cui, X. L.; Chen, B. L.; Xing, H. B. Energy-efficient separation alternatives: metal-organic frameworks and membranes for hydrocarbon separation. *Chem. Soc. Rev.* **2020**, *49*, 5359−5406.

(7) Han, X.; Yang, S. H. Molecular Mechanisms behind acetylene adsorption and selectivity in functional porous materials. *Angew. Chem., Int. Ed.* **2023**, *62*, No. e202218274.

(8) Li, Y. P.; Wang, Y.; Xue, Y. Y.; Li, H. P.; Zhai, Q. G.; Li, S. N.; Jiang, Y. C.; Hu, M. C.; Bu, X. H. Ultramicroporous building units as a path to bi-microporous metal-organic frameworks with high acetylene storage and separation performance. *Angew. Chem., Int. Ed.* **2019**, *58*, 13590−13595.
(9) Xu, T. T.; Jiang, Z. Z.; Liu, P. X.; Chen, H. N.; Lan, X. S.; Chen, D. L.; Li, L. B.; He, Y. B. Immobilization of oxygen atoms in the pores of microporous metal-organic frameworks for C_2H_2 separation and purification. *ACS Appl. Nano Mater.* **2020**, *3*, 2911−2919.
(10) Qian, Q.-L.; Gu, X.-W.; Pei, J. Y.; Wen, H.-M.; Wu, H.; Zhou, W.; Li, B.; Qian, G. D. A novel anion-pillared metal-organic framework for highly efficient separation of acetylene from ethylene and carbon dioxide. *J. Mater. Chem. A* **2021**, *9*, 9248−9255.
(11) Yang, S.-Q.; Krishna, R.; Chen, H.; Li, L.; Zhou, L.; An, Y.-F.; Zhang, F.-Y.; Zhang, Q.; Zhang, Y.-H.; Li, W.; Hu, T.-L.; Bu, X.-H. Immobilization of the polar group into an ultramicroporous metal-organic framework enabling benchmark inverse selective CO_2/C_2H_2 separation with record C_2H_2 production. *J. Am. Chem. Soc.* **2023**, *145*, 13901−13911.
(12) Wang, J. W.; Fan, S. C.; Li, H. P.; Bu, X. H.; Xue, Y. Y.; Zhai, Q. G. De-linker-enabled exceptional volumetric acetylene storage capacity and benchmark C_2H_2/C_2H_4 and C_2H_2/CO_2 separations in metal-organic frameworks. *Angew. Chem., Int. Ed.* **2023**, *62*, No. e202217839.
(13) Zhou, D.-D.; Zhang, J.-P. On the role of flexibility for adsorptive separation. *Acc. Chem. Res.* **2022**, *55*, 2966−2977.
(14) Shivanna, M.; Bezrukov, A. A.; Gascón-Pérez, V.; Otake, K.; Sanda, S.; O'Hearn, D. J.; Yang, Q.-Y.; Kitagawa, S.; Zaworotko, M. J. Flexible coordination network exhibiting water vapor-induced reversible switching between closed and open phases. *ACS Appl. Mater. Interfaces* **2022**, *14*, 39560−39566.
(15) Dong, Q. B.; Huang, Y. H.; Wan, J. M.; Lu, Z. Y.; Wang, Z. X.; Gu, C.; Duan, J. G.; Bai, J. F. Confining water nanotubes in a $Cu_{10}O_{13}$-based metal-organic framework for propylene/propane separation with record-high selectivity. *J. Am. Chem. Soc.* **2023**, *145*, 8043−8051.
(16) Wang, W. Z.; Wang, G. D.; Zhang, B.; Li, X. Y.; Hou, L.; Yang, Q. Y.; Liu, B. Discriminatory gate-opening effect in a flexible metal-organic framework for inverse CO_2/C_2H_2 separation. *Small* **2023**, *19*, No. 2302975.
(17) Li, L. Y.; Guo, L. D.; Zhang, Z. G.; Yang, Q. W.; Yang, Y. W.; Bao, Z. B.; Ren, Q. L.; Li, J. A robust squarate-based metal-organic framework demonstrates record-high affinity and selectivity for xenon over krypton. *J. Am. Chem. Soc.* **2019**, *141*, 9358−9364.
(18) Ye, Y. X.; Xian, S. K.; Cui, H.; Tan, K.; Gong, L. S.; Liang, B.; Pham, T.; Pandey, H.; Krishna, R.; Lan, P. C.; Forrest, K. A.; Space, B.; Thonhauser, T.; Li, J.; Ma, S. Q. Metal-organic framework based hydrogen-bonding nanotrap for efficient acetylene storage and separation. *J. Am. Chem. Soc.* **2022**, *144*, 1681−1689.
(19) Zhu, X. Q.; Ke, T.; Zhou, J. Y.; Song, Y. F.; Xu, Q. Q.; Zhang, Z. G.; Bao, Z. B.; Yang, Y. W.; Ren, Q. L.; Yang, Q. W. Vertex strategy in layered 2D MOFs: Simultaneous improvement of thermodynamics and kinetics for record C_2H_2/CO_2 separation performance. *J. Am. Chem. Soc.* **2023**, *145*, 9254−9263.
(20) Huang, X.; Jiang, S. Y.; Ma, D.; Xie, J.; Feng, X.; Wang, B. Molecular exclusion separation of 1-butene isomers by a robust metal-organic framework under humid conditions. *Angew. Chem., Int. Ed.* **2023**, *62*, No. e202303671.
(21) Zhang, L.; He, Z. Y.; Liu, Y. P.; You, J. J.; Lin, L.; Jia, J. H.; Chen, S.; Hua, N. B.; Ma, L.-A.; Ye, X. Y.; Liu, Y. R.; Chen, C.-X.; Wang, Q. T. A robust squarate-cobalt metal-organic framework for CO_2/N_2 separation. *ACS Appl. Mater. Interfaces* **2023**, *15*, 30394−30401.
(22) Wang, T.; Lin, E.; Peng, Y.-L.; Chen, Y.; Cheng, P.; Zhang, Z. J. Rational design and synthesis of ultramicroporous metal-organic frameworks for gas separation. *Coordin. Chem. Rev.* **2020**, *423*, No. 213485.
(23) Verma, G.; Ren, J. Y.; Kumar, S.; Ma, S. Q. New paradigms in porous framework materials for acetylene storage and separation. *Eur. J. Inorg. Chem.* **2021**, *2021*, 4498−4507.
(24) Wang, J.-X.; Liang, C.-C.; Gu, X.-W.; Wen, H.-M.; Jiang, C. H.; Li, B.; Qian, G. D.; Chen, B. L. Recent advances in microporous metal-organic frameworks as promising adsorbents for gas separation. *J. Mater. Chem. A* **2022**, *10*, 17878−17916.
(25) Dong, A.; Chen, D. D.; Li, Q. P.; Qian, J. J. Metal-organic frameworks for greenhouse gas applications. *Small* **2022**, *19*, No. 2201550.
(26) Idrees, K. B.; Chen, Z. J.; Zhang, X.; Mian, M. R.; Drout, R. J.; Islamoglu, T.; Farha, O. K. Tailoring pore aperture and structural defects in zirconium-based metal-organic frameworks for krypton/xenon separation. *Chem. Mater.* **2020**, *32*, 3776−3782.
(27) Chen, C. X.; Wei, Z. W.; Pham, T.; Lan, P. C.; Zhang, L.; Forrest, K. A.; Chen, S.; Al-Enizi, A. M.; Nafady, A.; Su, C. Y.; Ma, S. Q. Nanospace engineering of metal-organic frameworks through dynamic spacer installation of multifunctionalities for efficient separation of ethane from ethane/ethylene mixtures. *Angew. Chem., Int. Ed.* **2021**, *60*, 9680−9685.
(28) Kumar, N.; Mukherjee, S.; Harvey-Reid, N. C.; Bezrukov, A. A.; Tan, K.; Martins, V.; Vandichel, M.; Pham, T.; Van Wyk, L. M.; Oyekan, K.; Kumar, A.; Forrest, K. A.; Patil, K. M.; Barbour, L. J.; Space, B.; Huang, Y. N.; Kruger, P. E.; Zaworotko, M. J. Breaking the trade-off between selectivity and adsorption capacity for gas separation. *Chem.* **2021**, *7*, 3085−3098.
(29) Yu, L.; Han, X.; Wang, H.; Ullah, S.; Xia, Q. B.; Li, W. Y.; Li, J. N.; Da Silva, I.; Manuel, P.; Rudić, S.; Cheng, Y. Q.; Yang, S. H.; Thonhauser, T.; Li, J. Pore distortion in a metal-organic framework for regulated separation of propane and propylene. *J. Am. Chem. Soc.* **2021**, *143*, 19300−19305.
(30) Gaidimas, M. A.; Son, F. A.; Mian, M. R.; Islamoglu, T.; Farha, O. K. Influence of pore size on hydrocarbon transport in isostructural metal-organic framework crystallites. *Acs Appl. Mater. Interfaces* **2022**, *14*, 47222−47229.
(31) Macreadie, L. K.; Idrees, K. B.; Smoljan, C. S.; Farha, O. K. Expanding linker dimensionality in metal-organic frameworks for Sub-Ångstrom pore control for separation applications. *Angew. Chem., Int. Ed.* **2023**, *62*, No. e202304094.
(32) Wang, W.; Yang, H. J.; Chen, Y. C.; Bu, X. H.; Feng, P. Y. Cyclobutanedicarboxylate metal-organic frameworks as a platform for dramatic amplification of pore partition effect. *J. Am. Chem. Soc.* **2023**, *145*, 17551−17556.
(33) Chen, Z. J.; Mian, M. R.; Lee, S.-J.; Chen, H. Y.; Zhang, X.; Kirlikovali, K. O.; Shulda, S.; Melix, P.; Rosen, A. S.; Parilla, P. A.; Gennett, T.; Snurr, R. Q.; Islamoglu, T.; Yildirim, T.; Farha, O. K. Fine-tuning a robust metal-organic framework toward enhanced clean energy gas storage. *J. Am. Chem. Soc.* **2021**, *143*, 18838−18843.
(34) Zhang, Z. Q.; Peh, S. B.; Krishna, R.; Kang, C. J.; Chai, K. G.; Wang, Y. X.; Shi, D. C.; Zhao, D. Optimal pore chemistry in an ultramicroporous metal-organic framework for benchmark inverse CO_2/C_2H_2 separation. *Angew. Chem., Int. Ed.* **2021**, *60*, 17198−17204.
(35) Tan, Y. X.; Lin, J.; Li, Q. H.; Li, L. Q.; Anil Borse, R.; Lu, W. G.; Wang, Y. B.; Yuan, D. Q. Overcoming the trade-off between C_2H_2 sorption and separation performance by regulating metal-alkyne chemical interaction in metal-organic frameworks. *Angew. Chem., Int. Ed.* **2023**, *62*, No. e202302882.
(36) Guo, F. A.; Wang, J.; Chen, C. L.; Dong, X. L.; Li, X. Y.; Wang, H.; Guo, P.; Han, Y.; Li, J. Linker vacancy engineering of a robust ftw-type Zr-MOF for hexane isomers separation. *Angew. Chem., Int. Ed.* **2023**, *62*, No. e202303527.
(37) Zhang, L.; Qian, J. J.; Yang, W. B.; Kuang, X. F.; Zhang, J.; Cui, Y. X.; Wu, W. M.; Wu, X.-Y.; Lu, C.-Z.; Chen, W.-Z. A (3,8)-connected metal-organic framework with a unique binuclear $[Ni_2(\mu_2\text{-OH})(COO)_2]$ node for high H_2 and CO_2 adsorption capacities. *J. Mater. Chem. A* **2015**, *3*, 15399−15402.
(38) Fan, W. D.; Yuan, S.; Wang, W. J.; Feng, L.; Liu, X. P.; Zhang, X. R.; Wang, X.; Kang, Z. X.; Dai, F. N.; Yuan, D. Q.; Sun, D. F.; Zhou, H.-C. Optimizing multivariate metal-organic frameworks for efficient C_2H_2/CO_2 separation. *J. Am. Chem. Soc.* **2020**, *142*, 8728−8737.
(39) Feng, L.; Day, G. S.; Wang, K.-Y.; Yuan, S.; Zhou, H.-C. Strategies for pore engineering in zirconium metal-organic frameworks. *Chem.* **2020**, *6*, 2902−2923.

https://doi.org/10.1021/jacs.3c12032
J. Am. Chem. Soc. 2024, 146, 7341−7351

(40) Li, H.; Liu, C. P.; Chen, C.; Di, Z. Y.; Yuan, D. Q.; Pang, J. D.; Wei, W.; Wu, M. Y.; Hong, M. C. An unprecedented pillar-cage fluorinated hybrid porous framework with highly efficient acetylene storage and separation. *Angew. Chem., Int. Ed.* **2021**, *60*, 7547−7552.
(41) Zhang, L.; Li, F. F.; You, J. J.; Hua, N. B.; Wang, Q. T.; Si, J. H.; Chen, W. Z.; Wang, W. J.; Wu, X. Y.; Yang, W. B.; Yuan, D. Q.; Lu, C. Z.; Liu, Y. R.; Al-Enizi, A. M.; Nafady, A.; Ma, S. Q. A window-space-directed assembly strategy for the construction of supertetrahedron-based zeolitic mesoporous metal-organic frameworks with ultramicroporous apertures for selective gas adsorption. *Chem. Sci.* **2021**, *12*, 5767−5773.
(42) Shao, K.; Wen, H. M.; Liang, C. C.; Xiao, X. Y.; Gu, X. W.; Chen, B. L.; Qian, G. D.; Li, B. Engineering supramolecular binding sites in a chemically stable metal-organic framework for simultaneous high C_2H_2 storage and separation. *Angew. Chem., Int. Ed.* **2022**, *61*, No. e202211523.
(43) Yang, L. Z.; Xie, W. P.; Fu, Q. J.; Yan, L. T.; Zhang, S.; Jiang, H. M.; Li, L. J.; Gu, X.; Liu, D. D.; Dai, P. C.; Zheng, Q. B.; Zhao, X. B. Highly selective separation of C_2H_2/CO_2 and C_2H_2/C_2H_4 in an N-rich cage-based microporous metal-organic framework. *Adsorpt. Sci. Technol.* **2023**, *2023*, 1.
(44) Zhao, X.; Bu, X. H.; Zhai, Q.-G.; Tran, H.; Feng, P. Y. Pore space partition by symmetry-matching regulated ligand insertion and dramatic tuning on carbon dioxide uptake. *J. Am. Chem. Soc.* **2015**, *137*, 1396−1399.
(45) Zhao, X.; Bu, X. H.; Nguyen, E. T.; Zhai, Q.-G.; Mao, C. Y.; Feng, P. Y. Multivariable modular design of pore space partition. *J. Am. Chem. Soc.* **2016**, *138*, 15102−15105.
(46) Zhai, Q.-G.; Bu, X. H.; Zhao, X.; Li, D.-S.; Feng, P. Y. Pore space partition in metal-organic frameworks. *Acc. Chem. Res.* **2017**, *50*, 407−417.
(47) Li, J.; Chen, S.; Jiang, L. Y.; Wu, D. P.; Li, Y. S. Pore space partitioning of metal-organic framework for C_2H_x separation from methane. *Inorg. Chem.* **2019**, *58*, 5410−5413.
(48) Zhang, Q.; Yang, S. Q.; Zhou, L.; Yu, L.; Li, Z. F.; Zhai, Y. J.; Hu, T. L. Pore-space partition through an embedding metal-carboxylate chain-induced topology upgrade strategy for the separation of acetylene/ethylene. *Inorg. Chem.* **2021**, *60*, 19328−19335.
(49) Hong, Q. L.; Wang, W. J.; Chen, S. M.; Chen, K.; Liu, M.; Zhang, H.-X.; Zhang, J. Host-guest pore space partition in a boron imidazolate framework for ethylene separation. *Chem. Mater.* **2022**, *34*, 307−313.
(50) Hong, A. N.; Yang, H. J.; Bu, X. H.; Feng, P. Y. Pore space partition of metal-organic frameworks for gas storage and separation. *EnergyChem.* **2022**, *4*, No. 100080.
(51) Xiao, Y. C.; Chen, Y. C.; Wang, W.; Yang, H. J.; Hong, A. N.; Bu, X. H.; Feng, P. Y. Simultaneous control of flexibility and rigidity in pore-space-partitioned metal-organic frameworks. *J. Am. Chem. Soc.* **2023**, *145*, 10980−10986.
(52) Wang, Y.; Jia, X. X.; Yang, H. J.; Wang, Y. X.; Chen, X. T.; Hong, A. N.; Li, J. P.; Bu, X. H.; Feng, P. Y. A strategy for constructing pore-space-partitioned MOFs with high uptake capacity for C_2 hydrocarbons and CO_2. *Angew. Chem., Int. Ed.* **2020**, *59*, 19027−19030.
(53) Hong, A. N.; Wang, Y. X.; Chen, Y. C.; Yang, H. J.; Kusumoputro, E.; Bu, X. H.; Feng, P. Y. Concurrent enhancement of acetylene uptake capacity and selectivity by progressive core expansion and extra-framework anions in pore-space-partitioned metal-organic frameworks. *Chem.—Eur. J.* **2023**, *29*, No. e202203547.
(54) Ye, Y. X.; Ma, Z. L.; Lin, R.-B.; Krishna, R.; Zhou, W.; Lin, Q. J.; Zhang, Z. J.; Xiang, S. C.; Chen, B. L. Pore Space partition within a metal-organic framework for highly efficient C_2H_2/CO_2 separation. *J. Am. Chem. Soc.* **2019**, *141*, 4130−4136.
(55) Xue, Y. Y.; Bai, X. Y.; Zhang, J.; Wang, Y.; Li, S. N.; Jiang, Y. C.; Hu, M. C.; Zhai, Q. G. Precise pore space partitions combined with high-density hydrogen-bonding acceptors within metal-organic frameworks for highly efficient acetylene storage and separation. *Angew. Chem., Int. Ed.* **2021**, *60*, 10122−10128.
(56) Yang, H. J.; Chen, Y. C.; Dang, C.; Hong, A. N.; Feng, P. Y.; Bu, X. H. Optimization of pore-space-partitioned metal-organic frameworks using the bioisosteric concept. *J. Am. Chem. Soc.* **2022**, *144*, 20221−20226.
(57) Zhu, B. Y.; Cao, J.-W.; Mukherjee, S.; Pham, T.; Zhang, T.; Wang, T.; Jiang, X.; Forrest, K. A.; Zaworotko, M. J.; Chen, K.-J. Pore engineering for one-step ethylene purification from a three-component hydrocarbon mixture. *J. Am. Chem. Soc.* **2021**, *143*, 1485−1492.
(58) Hong, A. N.; Yang, H. J.; Li, T.; Wang, Y.; Wang, Y. X.; Jia, X. X.; Zhou, A.; Kusumoputro, E.; Li, J. P.; Bu, X. H.; Feng, P. Y. Pore-space partition and optimization for propane-selective high-performance propane/propylene separation. *ACS Appl. Mater. Interfaces* **2021**, *13*, 52160−52166.
(59) Xiao, Y. C.; Hong, A. N.; Chen, Y. C.; Yang, H. J.; Wang, Y. X.; Bu, X. H.; Feng, P. Y. Developing water-stable pore-partitioned metal-organic frameworks with multi-level symmetry for high-performance sorption applications. *Small* **2022**, *19*, No. 2205119.
(60) Chen, K.-J.; Scott, Hayley S.; Madden, D. G.; Pham, T.; Kumar, A.; Bajpai, A.; Lusi, M.; Forrest, K. A.; Space, B.; Perry, J.; John, J.; Zaworotko, M. J. Benchmark C_2H_2/CO_2 and CO_2/C_2H_2 separation by two closely related hybrid ultramicroporous materials. *Chem.* **2016**, *1*, 753−765.
(61) Cui, X. L.; Chen, K. J.; Xing, H. B.; Yang, Q. W.; Krishna, R.; Bao, Z. B.; Wu, H.; Zhou, W.; Dong, X. L.; Han, Y.; Li, Bin; Ren, Q. L.; Zaworotko, M. J.; Chen, B. L. Pore chemistry and size control in hybrid porous materials for acetylene capture from ethylene. *Science* **2016**, *353*, 141−144.
(62) Li, B.; Cui, X. L.; O'Nolan, D.; Wen, H.-M.; Jiang, M. D.; Krishna, R.; Wu, H.; Lin, R.-B.; Chen, Y.-S.; Yuan, D. Q.; Xing, H. B.; Zhou, W.; Ren, Q. L.; Qian, G. D.; Zaworotko, M. J.; Chen, B. L. An ideal molecular sieve for acetylene removal from ethylene with record selectivity and productivity. *Adv. Mater.* **2017**, *29*, No. 1704210.
(63) Lin, R.-B.; Li, L. B.; Wu, H.; Arman, H.; Li, B.; Lin, R.-G.; Zhou, W.; Chen, B. L. Optimized separation of acetylene from carbon dioxide and ethylene in a microporous material. *J. Am. Chem. Soc.* **2017**, *139*, 8022−8028.
(64) Belmabkhout, Y.; Zhang, Z. Q.; Adil, K.; Bhatt, P. M.; Cadiau, A.; Solovyeva, V.; Xing, H. B.; Eddaoudi, M. Hydrocarbon recovery using ultra-microporous fluorinated MOF platform with and without uncoordinated metal sites: I- structure properties relationships for C_2H_2/C_2H_4 and CO_2/C_2H_2 separation. *Chem. Eng. J.* **2019**, *359*, 32−36.
(65) Shivanna, M.; Otake, K.; Song, B. Q.; van Wyk, L. M.; Yang, Q. Y.; Kumar, N.; Feldmann, W. K.; Pham, T.; Suepaul, S.; Space, B.; Barbour, L. J.; Kitagawa, S.; Zaworotko, M. J. Benchmark acetylene binding affinity and separation through induced fit in a flexible hybrid ultramicroporous material. *Angew. Chem., Int. Ed.* **2021**, *60*, 20383−20390.
(66) Ebadi Amooghin, A.; Sanaeepur, H.; Luque, R.; Garcia, H.; Chen, B. L. Fluorinated metal-organic frameworks for gas separation. *Chem. Soc. Rev.* **2022**, *51*, 7427−7508.
(67) Jiang, Y. J.; Hu, Y. Q.; Luan, B. H.; Wang, L. Y.; Krishna, R.; Ni, H. F.; Hu, X.; Zhang, Y. B. Benchmark single-step ethylene purification from ternary mixtures by a customized fluorinated anion-embedded MOF. *Nat. Commun.* **2023**, *14*, 401.
(68) Zhang, L.; Yang, W. B.; Wu, X.-Y.; Lu, C.-Z.; Chen, W.-Z. A hydrophobic metal-organic framework based on cubane-type $[Co_4(\mu_3\text{-}F)_3(\mu_3\text{-}SO_4)]^{3+}$ clusters for gas storage and adsorption selectivity of benzene over cyclohexane. *Chem.—Eur. J.* **2016**, *22*, 11283−11290.
(69) Peng, Y.-L.; Pham, T.; Li, P. F.; Wang, T.; Chen, Y.; Chen, K.-J.; Forrest, K. A.; Space, B.; Cheng, P.; Zaworotko, M. J.; Zhang, Z. J. Robust ultramicroporous metal-organic frameworks with benchmark affinity for acetylene. *Angew. Chem., Int. Ed.* **2018**, *57*, 10971−10975.
(70) Liu, Y.; Liu, J. H.; Xiong, H. T.; Chen, J. W.; Chen, S. X.; Zeng, Z. L.; Deng, S. G.; Wang, J. Negative electrostatic potentials in a Hofmann-type metal-organic framework for efficient acetylene separation. *Nat. Commun.* **2022**, *13*, 5515.
(71) Pei, J. Y.; Shao, K.; Wang, J. X.; Wen, H. M.; Yang, Y.; Cui, Y. J.; Krishna, R.; Li, B.; Qian, G. D. A chemically stable hofmann-type metal-organic framework with sandwich-like binding sites for benchmark acetylene capture. *Adv. Mater.* **2020**, *32*, No. 1908275.

https://doi.org/10.1021/jacs.3c12032
J. Am. Chem. Soc. 2024, 146, 7341−7351

(72) Xie, X.-J.; Zeng, H.; Xie, M.; Chen, W.; Hua, G.-F.; Lu, W. G.; Li, D. A metal-organic framework for C_2H_2/CO_2 separation under highly humid conditions: Balanced hydrophilicity/hydrophobicity. *Chem. Eng. J.* **2022**, *427*, No. 132033.
(73) Luo, F.; Yan, C. S.; Dang, L. L.; Krishna, R.; Zhou, W.; Wu, H.; Dong, X. L.; Han, Y.; Hu, T.-L.; O'Keeffe, M.; Wang, L. L.; Luo, M. B.; Lin, R.-B.; Chen, B. L. UTSA-74: A MOF-74 isomer with two accessible binding sites per metal center for highly selective gas separation. *J. Am. Chem. Soc.* **2016**, *138*, 5678−5684.
(74) Niu, Z.; Cui, X. L.; Pham, T.; Verma, G.; Lan, P. C.; Shan, C.; Xing, H. B.; Forrest, K. A.; Suepaul, S.; Space, B.; Nafady, A.; Al-Enizi, A. M.; Ma, S. Q. A MOF-based ultra-strong acetylene nano-trap for highly efficient C_2H_2/CO_2 separation. *Angew. Chem., Int. Ed.* **2021**, *60*, 5283−5288.
(75) Chen, C.-X.; Pham, T.; Tan, K.; Krishna, R.; Lan, P. C.; Wang, L. F.; Chen, S. B.; Al-Enizi, A. M.; Nafady, A.; Forrest, K. A.; Wang, H. P.; Wang, S. C.; Shan, C.; Zhang, L.; Su, C.-Y.; Ma, S. Q. Regulating C_2H_2/CO_2 adsorption selectivity by electronic-state manipulation of iron in metal-organic frameworks. *Cell Rep. Phys. Sci.* **2022**, *3*, No. 100977.
(76) Gao, J. K.; Qian, X. F.; Lin, R. B.; Krishna, R.; Wu, H.; Zhou, W.; Chen, B. L. Mixed metal-organic framework with multiple binding sites for efficient C_2H_2/CO_2 separation. *Angew. Chem., Int. Ed.* **2020**, *59*, 4396−4400.
(77) Zhang, L.; Jiang, K.; Yang, L. F.; Li, L. B.; Hu, E.; Yang, L.; Shao, K.; Xing, H. B.; Cui, Y. J.; Yang, Y.; Li, B.; Chen, B. L.; Qian, G. D. Benchmark C_2H_2/CO_2 separation in an ultra-microporous metal-organic framework via copper(I)-alkynyl chemistry. *Angew. Chem., Int. Ed.* **2021**, *60*, 15995−16002.
(78) Meng, L. K.; Yang, L. X.; Chen, C. L.; Dong, X. L.; Ren, S. Y.; Li, G. H.; Li, Y.; Han, Y.; Shi, Z.; Feng, S. H. Selective acetylene adsorption within an imino-functionalized nanocage-based metal-organic framework. *ACS Appl. Mater. Interfaces* **2020**, *12*, 5999−6006.
(79) Zeng, H.; Xie, M.; Huang, Y. L.; Zhao, Y. F.; Xie, X. J.; Bai, J. P.; Wan, M. Y.; Krishna, R.; Lu, W. G.; Li, D. Induced fit of cinduced fit of C_2H_2 in aflexible MOF through cooperative action of open metal sites C_2H_2 in a flexible MOF through cooperative action of open metal sites. *Angew. Chem., Int. Ed.* **2019**, *58*, 8515−8519.
(80) Pei, J. Y.; Wen, H. M.; Gu, X. W.; Qian, Q. L.; Yang, Y.; Cui, Y. J.; Li, B.; Chen, B. L.; Qian, G. D. Dense packing of acetylene in a stable and low-cost metal-organic framework for efficient C_2H_2/CO_2 separation. *Angew. Chem., Int. Ed.* **2021**, *60*, 25068−25074.

https://doi.org/10.1021/jacs.3c12032
J. Am. Chem. Soc. 2024, 146, 7341−7351